Journal of Rock Mechanics and Geotechnical Engineering 8 (2016) 462–471

Contents lists available at ScienceDirect

Journal of Rock Mechanics and Geotechnical Engineering

journal homepage: www.rockgeotech.org

Full length article

Characterization of transient groundwater flow through a high arch dam foundation during reservoir impounding

Yifeng Chen [a], Jiamin Hong [a], Shaolong Tang [b], Chuangbing Zhou [a,b,*]

[a] State Key Laboratory of Water Resources and Hydropower Engineering Science, Wuhan University, Wuhan 430072, China
[b] School of Civil Engineering and Architecture, Nanchang University, Nanchang 330031, China

ARTICLE INFO

Article history:
Received 19 November 2015
Received in revised form
31 January 2016
Accepted 30 March 2016
Available online 15 May 2016

Keywords:
Jinping I arch dam
Inverse modeling
Hydraulic conductivity
Fractured rock
Groundwater flow
Seepage control

ABSTRACT

Even though a large number of large-scale arch dams with height larger than 200 m have been built in the world, the transient groundwater flow behaviors and the seepage control effects in the dam foundations under difficult geological conditions are rarely reported. This paper presents a case study on the transient groundwater flow behaviors in the rock foundation of Jinping I double-curvature arch dam, the world's highest dam of this type to date that has been completed. Taking into account the geological settings at the site, an inverse modeling technique utilizing the time series measurements of both hydraulic head and discharge was adopted to back-calculate the permeability of the foundation rocks, which effectively improves the uniqueness and reliability of the inverse modeling results. The transient seepage flow in the dam foundation during the reservoir impounding was then modeled with a parabolic variational inequality (PVI) method. The distribution of pore water pressure, the amount of leakage, and the performance of the seepage control system in the dam foundation during the entire impounding process were finally illustrated with the numerical results.

1. Introduction

Over the last two decades, tens of large-scale arch dams, typically with a height over 200 m, have been designed and/or constructed over deeply cut narrow valleys in southwestern China, such as Ertan (Zhou et al., 2008), Xiaowan (Chai et al., 2004; Lin et al., 2015), Xiluodu (Liu et al., 2013; Fan et al., 2015), Jinping I (Fei et al., 2010; Chen et al., 2015, 2016) and Dagangshan (Zhang et al., 2015) arch dams, to name only a few. Owing to its thin structure, a high arch dam commonly suffers from a high pore water pressure (over 2 MPa) and a large pressure difference in the foundation rocks. Consequently, groundwater leakage, seepage erosion and/or abnormal distribution of uplift pressure frequently occur as a result of insufficient characterization of site conditions and/or improper design of seepage control systems (e.g. Chen et al., 2016). A proper characterization of the permeability of foundation rocks is therefore indispensable (Chen et al., 2010), either based on the site characterization data at the design stage, or based on the field measurement data at the impounding and operation stages, as a key step to better understand and control the groundwater flow behaviors in the dam foundations. To the best of our knowledge, however, a systematic study on the behaviors of transient groundwater flow and the effects of seepage control in a high arch dam foundation under difficult geological conditions has not yet been reported.

This study takes the Jinping I double-curvature arch dam, located in the middle reach of Yalong River, as an example to examine the transient groundwater flow behaviors in the high arch dam foundation. The Jinping I arch dam was completed in December 2013, with a maximum height of 305 m. The impounding of the reservoir began in November 2012, which was separated into four stages (Stages I–IV). In the second stage of reservoir impounding, however, a significant amount of leakage was observed from the drainage holes drilled in the lowest drainage tunnel at the left bank abutment at an elevation of 1595 m. Chen et al. (2016) comprehensively examined the source of leaking, the groundwater flow paths, the performance of grouting curtains, and the effects of engineering treatments of the leakage event on the dam safety by proposing a multi-objective inverse modeling procedure using the in-situ time series measurements of both flow rate and hydraulic head, together with the observations by water chemical analysis, digital borehole imaging and tunnel geological mapping. The transient groundwater flow behaviors in the dam foundation, however, remain to be further investigated. This study

* Corresponding author. Tel./fax: +86 27 68774295.
E-mail address: cbzhou@whu.edu.cn (C. Zhou).

Peer review under responsibility of Institute of Rock and Soil Mechanics, Chinese Academy of Sciences.

http://dx.doi.org/10.1016/j.jrmge.2016.03.004

aims to present the back-calculated permeability of the foundation rocks, the performance of the seepage control systems and the seepage flow behaviors in the Jinping I dam foundation.

2. Site characterization

2.1. Project description

The Jinping I double-curvature arch dam, located on the border between Muli and Yanyuan counties (Sichuan Province, China), is the first level of the cascade of dams in the middle reach of Yalong River. This dam has a maximum height of 305 m and a varying width of 63–16 m from the base to the crest. The dam is a major component of the hydraulic structures in the Jinping I Hydropower Project mainly designed for energy production, sediment trapping and flood control. Fig. 1 shows the layout of the project. The underground powerhouse cavern system is located in the right bank of the mountain about 350 m downstream the dam axis, with a total installed capacity of 3600 MW. The reservoir capacity is about 7.76×10^9 m^3 at the normal pool level of 1880 m.

The river course at the construction site was blocked on December 4, 2006 for the construction of the dam. The excavation of dam foundation started in August 2007 and was completed in September 2009. The first bucket of concrete was poured into the foundation on October 23, 2009, and the construction duration lasted for 50 months. The impounding of the reservoir began on November 30, 2012, and the reservoir water level was gradually elevated to the normal pool level (1880 m) by about 232 m in 21 months, which could be separated into four stages (stages I–IV), as shown in Fig. 2.

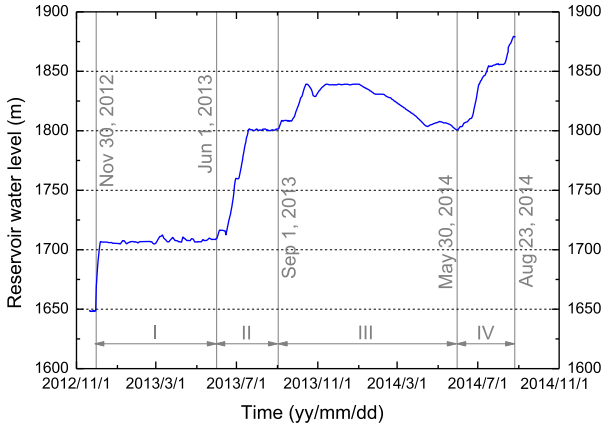

Fig. 2. The reservoir impounding process.

2.2. Geological settings

The Jinping I dam is located in a typical deeply cut V-shaped valley. As shown in Fig. 3, the dam foundation consists of a series of epizonal metamorphic rocks, which belong to the second member (T^2_{2-3z}) and the third member (T^3_{2-3z}) of the Zagunao group of upper to middle Triassic system ($T_{2\text{-}3z}$) (Qi et al., 2004). The rocks in the second member (from $T^{2(1)}_{2-3z}$ to $T^{2(8)}_{2-3z}$), on which the dam foundation is mostly situated, mainly consist of marble, breccia marble, lens of calcareous tuff phyllite and green schist. The third member (from $T^{3(1)}_{2-3z}$ to $T^{3(6)}_{2-3z}$), outcropping at higher elevation in the left bank slope, consists of slate and metamorphosed sandstone. The strata strike almost parallel to the river (N0°–30°E), dipping 25°–45° toward NW.

Several large-scale faults are developed at the dam site, including F_2, F_5 and F_8 in the left bank and F_{13} and F_{14} in the right bank (Fig. 3). Fault F_2, striking N30°–40°E and dipping 40°–56° toward NW, was formed as an associated structure of the shear zone in the second member ($T^{2(6)}_{2-3z}$) of the regional strata. It is about 0.2–0.8 m in thickness and mainly composed of schistose, cataclastic or mylonitic rocks. Faults F_{13} and F_{14}, striking with an angle about 50° to the axis of the machine hall and dipping 60°–80° toward S20°–30°E, are less permeable than the surrounding rocks, acting as low-permeability barriers to the groundwater movement. Besides the geological structures mentioned above, there are

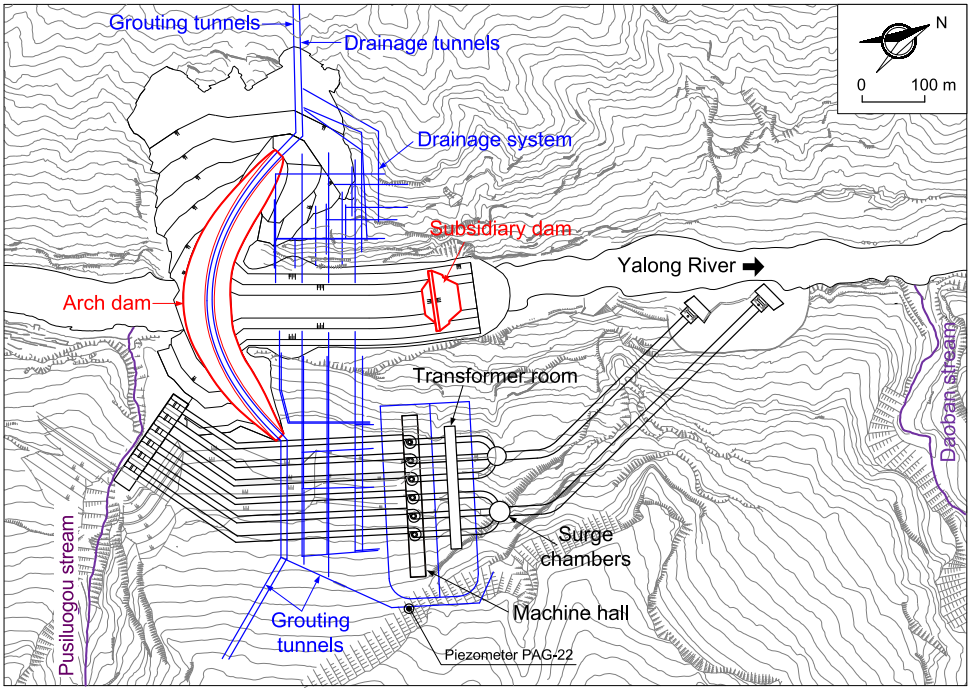

Fig. 1. Layout of the Jinping I Hydropower Project.

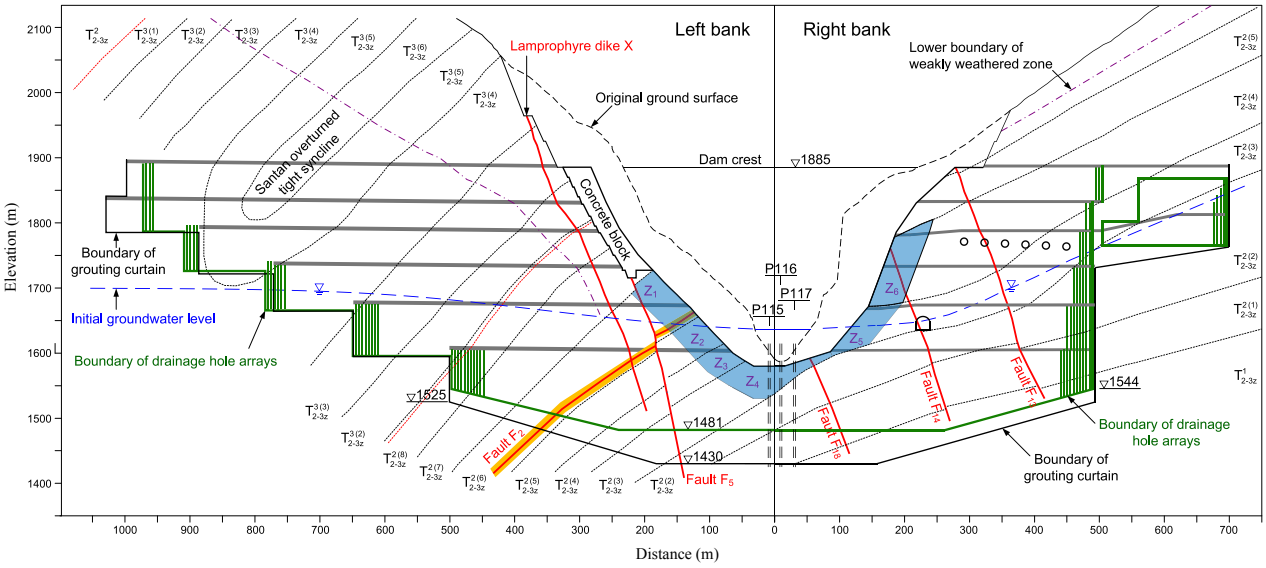

Fig. 3. Geological cross-section along the grouting curtain of the arch dam.

five sets of critically oriented joints developed at the dam site, with their preferential orientations being: (1) N15°–80°E/NW∠25°–45°; (2) N50°–70°E/SE∠50°–80°; (3) SN–N30°E/SE∠60°–80°; (4) N60°W–EW/NE∠60°–80°; and (5) N30°–50°W/NE∠60°–80°. Interested readers may refer to Chen et al. (2015, 2016) and Qi et al. (2004) for more details of the geological settings.

To evaluate the permeability of the foundation rocks, a large number of borehole packer tests were carried out at the dam site. Owing to the presence of intensely developed release fractures and the Santan overturned tight syncline (Fig. 3), the permeability of the rock masses in the left bank slope is generally larger than that in the right bank slope. The results of the packer tests also show that the permeability of the foundation rocks reduces with the increase of both vertical and horizontal distances from the slope surface (except in the deep crack zones (Qi et al., 2004)), due mainly to sparser release fractures, lower weathering degree and higher in-situ geostress at greater depths (Chen et al., 2015).

Long-term groundwater observations showed that the groundwater level in the left bank slope was relatively low before impounding, only slightly higher than the riverbed water level and with a gradient of about 4% discharging to the Yalong River (Fig. 3). On the contrary, the right bank slope at the dam site is rich in groundwater, which is recharged from a regional-scale fault (i.e. Jinping Mountain Fault) about 2 km east from the dam site. Therefore, the groundwater level in the right bank slope was much high before construction of the dam and was less influenced by the reservoir impounding.

2.3. Seepage control system

In order to lower the phreatic surface and reduce the pore water pressure at the dam foundation and its abutments, a large-scale seepage control system was constructed at the dam site. It consists of grouting curtains, drainage tunnels and drainage hole arrays, as shown in Figs. 1 and 3. The grouting curtains were constructed from six layers of grouting tunnels at both banks at the elevations of 1885 m, 1829 m, 1778 m, 1730 m, 1670 m and 1601 m, respectively. As shown in Fig. 3, the curtain was extended downwards to about 1430 m in the dam foundation, reaching the bedrocks with a permeability rate smaller than 1 Lu and cutting off the potential leakage paths under the dam foundation. The depth of the grouting curtain in both abutments was gradually reduced with the increase of the horizontal depth from the slope surface. Besides, a grouting curtain parallel to the river direction was also constructed in the right bank mountain to limit the groundwater flow into the underground caverns. The grouting curtains were spatially linked together to form a seepage-proof system of good integrity.

Moreover, thousands of drainage holes of about 110 mm in diameter and 3 m in spacing were drilled from the drainage tunnels constructed at elevations of 1829 m, 1785 m, 1730 m, 1670 m, and 1595 m, about 11.5 m downstream of the grouting curtains. Furthermore, five layers of drainage tunnels were constructed in the massive concrete blocks in both banks for stabilizing the abutments, and another three layers of drainage tunnels were excavated around the machine hall and the transformer room. The drainage holes were drilled downwards from the lowest drainage tunnels and upwards from the rest drainage tunnels.

2.4. Monitoring system

A groundwater monitoring system was implemented in the dam foundation for monitoring the real-time operation of the seepage control system and the groundwater flow behaviors. It includes 40 piezometers and 12 weirs installed in the drainage and grouting tunnels in the dam foundation. The piezometers, numbered from P2 to P13, are located at the left abutment, and the ones numbered from P13 to P22 are located at the right abutment. Most of the piezometers were installed 1–3 m below the concrete–rock interfaces. The weirs were installed at the outer ends of the drainage tunnels near the dam foundation for measuring the seepage flow rates out of the drainage system. Particularly, the discharge to the drainage tunnel at 1595 m at the left abutment from chainage k0 + 000 m to k0 + 226 m was measured by weir WEDB-3, and that at the same elevation at the right abutment was measured by weir WEDB-4. The locations of piezometers and weirs are shown in Fig. 4.

3. Numerical simulation and inverse modeling

3.1. Groundwater flow model

Given the relatively intensive discontinuities at the site and the scale of the dam and its foundation, this study adopted the equivalent continuum approach for assessment of the behaviors of the

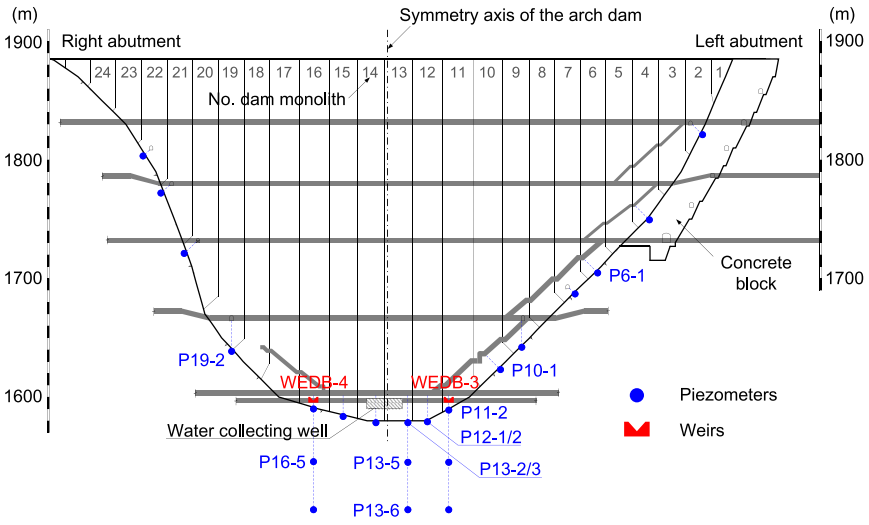

(a) Upstream view.

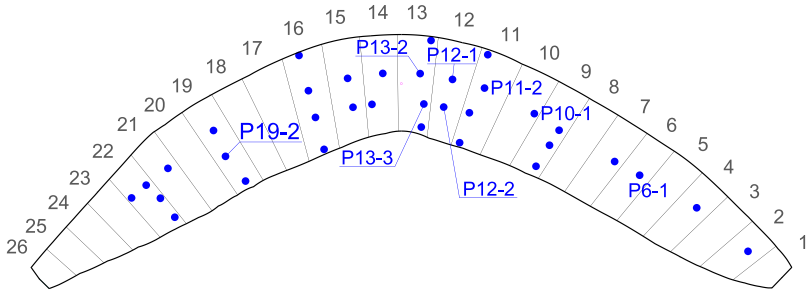

(b) Bird view.

Fig. 4. Locations of piezometers and weirs.

transient groundwater flow and the effects of the seepage control system on the Jinping I arch dam foundation. A large number of numerical algorithms have been developed to solve the transient groundwater flow problem (Karahan and Ayvaz, 2005a). In this study, the parabolic variational inequality (PVI) formulation proposed by Chen et al. (2011) was employed for modeling the transient flow in the dam foundation during the impounding process. Together with the borehole packer test results, the permeability of the foundation rocks was determined by an inverse modeling procedure that utilized the in-situ time series measurements of flow rate and hydraulic head for improving the reliability of the inverse results (Zhou et al., 2015; Chen et al., 2016). The numerical procedure has been implemented in the finite element code THYME3D (Chen et al., 2009), which has been widely applied in groundwater flow simulations in numerous large-scale hydropower projects (e.g. Chen et al., 2011, 2015, 2016; Li et al., 2014; Zhou et al., 2015; Wang et al., 2016).

3.2. Finite element mesh

A three-dimensional (3D) finite element mesh containing 2,575,234 brick elements (with some of them degenerated to tetrahedral elements) and 792,342 nodes was generated for simulation of the groundwater flow through the dam foundation, as shown in Fig. 5. The mesh has a rectangular base of 2300 m long along the river flow direction and 1850 m wide in another horizontal direction perpendicular to the river. The hydraulic structures, such as the diversion tunnel, the double-curvature arch dam and the underground caverns were all well represented. The drainage holes in the seepage control systems were modeled with a substructure technique (Chen et al., 2008, 2011) for accurately characterizing their boundary conditions and reducing the difficulty in mesh generation. The geological settings (such as the strata, faults and dike) and the grouting curtains were also well represented with brick elements.

3.3. Initial and boundary conditions

According to the impounding schedule of the reservoir, numerical simulations of the transient seepage flow at the dam site started at 8:00 on November 22, 2012 and ended at 8:00 on August 26, 2014. Given the rising rate of the reservoir water level, the time step length was taken as 3 days. The initial distribution of hydraulic head was determined with a steady-state seepage analysis by taking into account the hydrological conditions at the dam site before impounding.

The boundary conditions were specified as follows. The reservoir water level was specified on the upstream surface of the dam and the ground surface submerged in the reservoir according to the impounding process of the reservoir (Fig. 2). Similarly, the downstream surface of the subsidiary dam and the ground surface submerged in the downstream river channel were prescribed with the corresponding water level, which fluctuated around 1640 m. The base of the model and the transverse lateral boundaries (*ABFE* and *DCGH* in Fig. 5) were assumed to be impermeable. The drainage holes drilled downwards in the lowest drainage tunnel were imposed with a hydraulic head equal to the floor elevation of the connected drainage tunnel. The remaining drainage holes, the ground and dam surfaces above the upstream and downstream water levels and the boundaries of the drainage tunnels were all

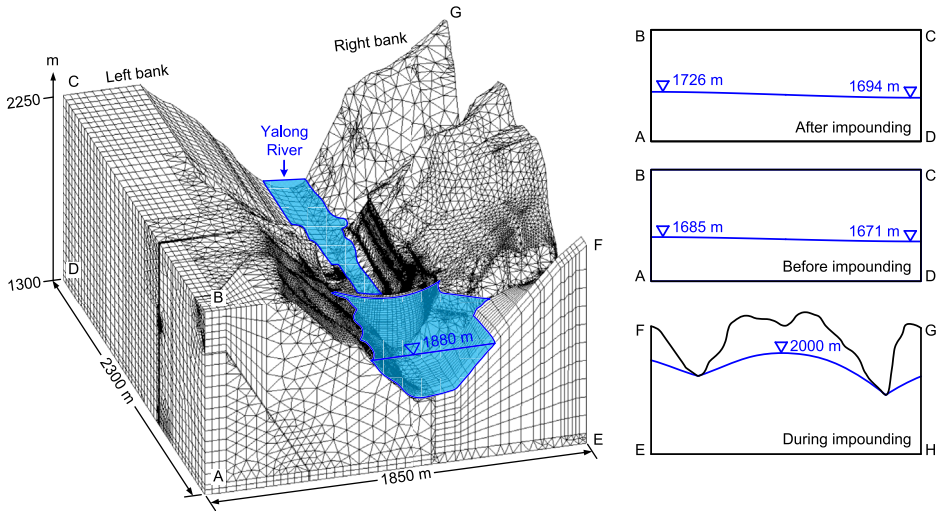

Fig. 5. 3D finite element mesh for the arch dam and the specified boundary conditions.

taken as the potential seepage boundaries satisfying the Signorini's complementary condition (Chen et al., 2008, 2011).

The boundary conditions on the mountain sides of the model (*ABCD* and *EFGH* in Fig. 5) were roughly determined according to the hydrogeological conditions at the dam site. As mentioned before, the groundwater level on the mountain side in the right bank slope (*EFGH* in Fig. 5) is much higher because of the groundwater recharged from the Jinping Mountain Fault, and it is less influenced by the reservoir impounding, as evidenced by the readings (about 1870 m) of piezometer PAG-22 located at the grouting tunnel around the underground powerhouse (Fig. 1). Taking into account the distance from the piezometer PAG-22 to the mountain side boundary of the model and the boundary conditions of the Pusiluogou stream and the Daoban stream, the distribution of groundwater level on this boundary could be well represented by a parabolic curve, with its maximum level being about 2000 m, as shown in Fig. 5.

On the contrary, the groundwater level in the left bank was rather low before impounding, and it is remarkably influenced by the reservoir impounding process. This boundary condition was assessed by inverse modeling (Chen et al., 2016), assuming that the groundwater level follows a modified trigonometric curve and varies linearly with the reservoir water level. The results were adopted in this study. Although the above lateral boundary conditions were specified with lower confidence based on the limited observations in the far field, the possible error was expected to have a secondary influence on the near-field groundwater flow in the dam foundation.

3.4. Hydraulic conductivities of the foundation rocks

Determination of the hydraulic parameters of the foundation rocks is the key to reliably characterizing the groundwater flow behaviors and assessing the seepage control effects in the dam foundation. The borehole packer test results are the main source for evaluating the permeability of the rock masses at the dam site. The packer tests, however, only evaluate the magnitude, rather than the anisotropy, of the hydraulic properties of rocks (Chen et al., 2016). The Lugeon values of the packer tests often vary dramatically from segment to segment in the boreholes and are less reliable (or even failure) as the tested rocks become more fractured and permeable, rendering the data less representative (Zhou et al., 2015). Furthermore, the packer tests were normally conducted before the foundation excavation and treatment, being not able to account for the excavation-induced permeability variation in the foundation rocks (Li et al., 2014; Chen et al., 2015, 2016). To overcome the limitations of the packer tests, inverse modeling could be applied by utilizing the field measurement data of groundwater for more reliably and representatively evaluating the permeability of the near-field foundation rocks.

Given that the foundation rocks at smaller depths generally exhibit a wider range of permeability (Fig. 6) and affect more the groundwater flow behaviors in the dam foundation, six zones (marked by Z_i, $i = 1$–6) of the foundation rocks in different rock formations near the excavation surface were selected for back calculation of their hydraulic conductivity. For convenience, we use a vector $\boldsymbol{K} = \{k_1, k_2, \ldots, k_6\}$ to denote the effective hydraulic conductivities of the zones yet to be back-calculated, in which k_i is the hydraulic conductivity of zone Z_i (assumed to be isotropic for simplicity). The inverse modeling procedure for estimation of the hydraulic conductivities will be presented in the next section.

Chen et al. (2016) showed that the two groups of subvertically oriented fractures extending along the river direction were well developed in the rock formations $T_{2-3z}^{2(6-8)}$ in the left bank abutment (Fig. 3), which were most likely formed as an associated structure of the Santan overturned tight syncline. The two groups of fractures are the major concentrated flow channels for the significant amount of groundwater leakage into the drainage tunnel at the elevation of 1595 m. The hydraulic conductivity tensors of the rock formations have been back-calculated and the anisotropy of the hydraulic properties of the rock masses has been clarified (Chen et al., 2016).

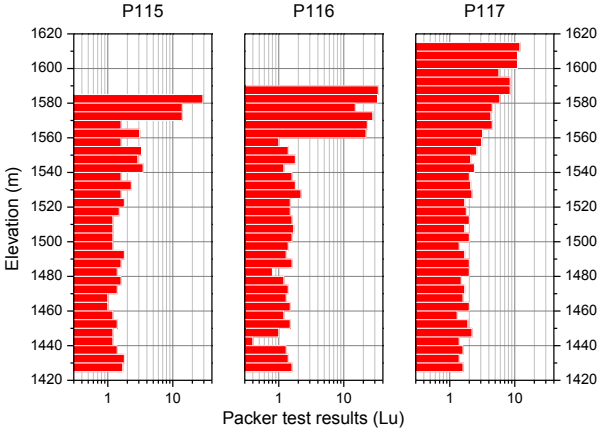

Fig. 6. Packer test results at three boreholes (with their locations shown in Fig. 3).

The inverse results were used in this study, as listed in Table 1. The hydraulic conductivities of the remaining rock units, faults and dike were evaluated by the numerous borehole packer tests performed on the corresponding rock units, as listed in Table 2. Other hydraulic parameters (i.e. the gravitational specific yield and the specific storage) that appear in the transient flow model are not involved in the back analysis for their relatively small uncertainty and limited impacts on the seepage field at a sufficiently low filling rate of the reservoir, with their values also given in Table 2.

3.5. Inverse modeling technique

The inverse calculations of aquifer parameters were frequently performed based on the field measurements of hydraulic head and/or the measurements at a steady state (e.g. Yang et al., 2004; Karahan and Ayvaz, 2005b, 2008; Garcia and Shigidi, 2006; Hernandez et al., 2006; Ayvaz et al., 2007; Chang et al., 2008; Virbulis et al., 2013), probably because of cheaper acquisition of such kind of data and easier implementation of the inverse models. The inverse solutions, however, may be plagued with the non-uniqueness problems (Mao et al., 2013). To overcome this limitation, Zhou et al. (2015) and Chen et al. (2016) proposed an inverse modeling procedure for reliably evaluating the permeability of the foundation rocks by defining one or two objective functions using the in-situ time series measurements of both discharge and hydraulic head. The procedure takes advantage of the orthogonal design, finite element forward modeling of the transient groundwater flow, artificial neural network and genetic algorithm, hence significantly reducing the computational cost and improving the reliability of the inverse results. In this study, the inverse modeling procedure was adopted, with the objective function defined as follows:

$$\min f(\boldsymbol{K}) = \sum_{i=1}^{M} \frac{\left\|\boldsymbol{\phi}_i(\boldsymbol{K}) - \boldsymbol{\phi}_i^{\mathrm{m}}\right\|_2^2}{\dim \boldsymbol{\phi}_i} + w \sum_{i=1}^{N} \frac{\left\|\boldsymbol{Q}_i(\boldsymbol{K}) - \boldsymbol{Q}_i^{\mathrm{m}}\right\|_2^2}{\dim \boldsymbol{Q}_i} \qquad (1)$$

where $\boldsymbol{K}$ is the hydraulic conductivities of the six foundation zones yet to be back-calculated; M is the number of piezometers; $\boldsymbol{\phi}_i^{\mathrm{m}}$ and $\boldsymbol{\phi}_i$ are the time series measurements of hydraulic head and the corresponding numerical results at piezometer i, respectively; N is the number of weirs or flowmeters; $\boldsymbol{Q}_i^{\mathrm{m}}$ and $\boldsymbol{Q}_i$ are the time series measurements of flow rate and the numerical results at weir i, respectively; $||\cdot||_2$ and $\dim(\cdot)$ denote the Euclidean norm and the dimension of a vector, respectively; and w is the weight coefficient to ensure a balance between the relative errors of the hydraulic head and flow rate measurements.

In this study, the time series measurements of the hydraulic head at piezometers P6-1, P10-1, P11-2, P12-1, P12-2, P13-2, P13-3, P13-5, P13-6, P16-6 and P19-2 in the dam foundation and the discharges out of the drainage tunnels at the elevation of 1595 m at both bank abutments were chosen for construction of the objective function, which measures the deviation between the observed and simulated results. Influenced by the performance of the sensors and the construction process, some unreliable (or unavailable) data were excluded.

The inverse modeling procedure involves the following four key components (Zhou et al., 2015; Chen et al., 2016): (1) A small set of representative parameter combinations is determined using the orthogonal design method within the possible ranges of the hydraulic conductivity parameters yet to be back-calculated; (2) The forward modeling of the transient seepage flow is invoked for each of the hydraulic conductivity combinations and the corresponding simulation results at the monitoring points are then obtained; (3) The implicit mapping from the parameter space (together with other input information to the finite element model, especially the time series data of reservoir water level) to the simulation results at the monitoring points is established by constructing and training a back propagation neural network (BPNN) model; and (4) A globally optimal parameter combination is finally obtained by using a genetic algorithm to minimize the objective function such that a good agreement is ensured between the field measurements and the numerical results calculated by the trained BPNN. This procedure not only makes tractable the large-scale inverse problems in engineering practices, but also significantly improves the reliability of the inverse solutions.

In this study, the orthogonal table, $L_{81}(9^6)$, was used to produce a set of 81 hydraulic conductivity combinations for finite element forward modeling of the transient groundwater flow through the dam foundation. A BPNN model with 7 neurons in the input layer, 18 and 24 neurons in the two hidden layers, and 13 neurons in the output layer was then constructed and trained with the data set composed of the hydraulic conductivity combinations, the time series data of reservoir water level and the simulation results at the monitoring points. The sigmoid function was selected as the transfer function of the BPNN model and the Levenberg–Marquardt back-propagation algorithm combined with Bayesian regularization was adopted for training of the model. Considering the magnitude of the square error term of hydraulic head and discharge in the objective function (Eq. (1)), a value of $w = 100$ was suggested for the weight coefficient.

4. Numerical results

4.1. The inverse modeling results

Table 3 lists the back-calculated hydraulic conductivities of the foundation rocks. The inverse results show that the hydraulic conductivity of the foundation rocks near the excavation surface is in the magnitude of (2–9) $\times$ 10^{-5} cm/s, which is in general remarkably higher than that of the deep-seated rocks in the same rock units. The results further show that the hydraulic conductivity of the rock masses decreases as the elevation decreases (i.e. lower at the dam foundation and higher at the dam abutments), owing mainly to the development of the release fractures and the influence of the in-situ stresses. Furthermore, it is interesting to note that the back-calculated hydraulic conductivity (7.2 $\times$ 10^{-5} cm/s) of zone Z_1 in

Table 1
Hydraulic conductivity tensors of rock formations $T_{2-3z}^{2(6)}$, $T_{2-3z}^{2(7)}$, and $T_{2-3z}^{2(8)}$ in the left bank (after Chen et al., 2016).

Rock formation	Hydraulic conductivity tensor (cm/s)			Principal value (cm/s)	Principal direction
$T_{2-3z}^{2(6)}$	7.02×10^{-5}	-2.00×10^{-5}	-9.04×10^{-7}	8.14×10^{-5}	S58°W∠30°
	-2.00×10^{-5}	2.61×10^{-5}	-1.86×10^{-5}	6.88×10^{-5}	N20°E∠54°
	-9.04×10^{-7}	-1.86×10^{-5}	6.64×10^{-5}	1.25×10^{-5}	S43°E∠18°
$T_{2-3z}^{2(7)}$	1.10×10^{-4}	-1.15×10^{-5}	2.51×10^{-7}	1.11×10^{-4}	S35°W∠04°
	-1.15×10^{-5}	1.35×10^{-5}	-5.49×10^{-6}	9.96×10^{-5}	N5°W∠84°
	2.51×10^{-7}	-5.49×10^{-6}	9.93×10^{-5}	1.18×10^{-5}	S55°E∠04°
$T_{2-3z}^{2(8)}$	1.37×10^{-4}	-4.36×10^{-6}	4.79×10^{-6}	1.38×10^{-4}	S30°W∠12°
	-4.36×10^{-6}	2.41×10^{-5}	-2.85×10^{-6}	1.14×10^{-4}	N22°E∠78°
	4.79×10^{-6}	-2.85×10^{-6}	1.15×10^{-4}	2.38×10^{-5}	S60°E∠02°

Table 2
Hydraulic properties of foundation rocks, grouting curtain and concrete.

Material	Permeability (cm/s)	Specific yield	Specific storage (m^{-1})	Material	Permeability (cm/s)	Specific yield	Specific storage (m^{-1})
Mass concrete	1×10^{-7}	0.002	3×10^{-7}	$T_{2-3z}^{2(4-5)}$ (in the left bank)	1.2×10^{-5}	0.025	2.5×10^{-6}
Concrete lining	1×10^{-6}	0.003	5×10^{-7}	$T_{2-3z}^{2(6)}$ (in the left bank)	–	0.025	2.5×10^{-6}
Grouting curtain	3.2×10^{-6}	0.003	5×10^{-7}	$T_{2-3z}^{2(7)}$ (in the left bank)	–	0.025	2.5×10^{-6}
Lamprophyre dike X	2×10^{-5}	0.05	5×10^{-6}	$T_{2-3z}^{2(8)}$ (in the left bank)	–	0.025	2.5×10^{-6}
Weakly weathered rock	2.5×10^{-4}	0.08	8×10^{-6}	$T_{2-3z}^{3(1-3)}$ (in the left bank)	3.5×10^{-5}	0.025	2.5×10^{-6}
Faults F_2, F_5	1.5×10^{-4}	0.07	7×10^{-6}	$T_{2-3z}^{3(4-6)}$ (in the left bank)	4×10^{-5}	0.03	3×10^{-6}
Faults F_{13}, F_{14}, F_{18}	2×10^{-5}	0.05	5×10^{-6}	$T_{2-3z}^{2(3)}$ (in the right bank)	3×10^{-5}	0.025	2.5×10^{-6}
T_{2-3z}^{1}	0.5×10^{-5}	0.02	2×10^{-6}	$T_{2-3z}^{2(4)}$ (in the right bank)	5×10^{-5}	0.025	2.5×10^{-6}
$T_{2-3z}^{2(1)}$	0.6×10^{-5}	0.02	2×10^{-6}	$T_{2-3z}^{2(5)}$ (in the right bank)	8×10^{-5}	0.025	2.5×10^{-6}
$T_{2-3z}^{2(2)}$	0.8×10^{-5}	0.02	2×10^{-6}	$T_{2-3z}^{2(6)}$ (in the right bank)	1.2×10^{-4}	0.03	3×10^{-6}
$T_{2-3z}^{2(3)}$ (in the left bank)	1×10^{-5}	0.025	2.5×10^{-6}				

the rock formation $T_{2-3z}^{2(6)}$ at the left bank abutment is completely consistent with the inverse result (see Table 1) previously obtained by Chen et al. (2016). Compared with the borehole packer test results plotted in Fig. 6, however, the back-calculated hydraulic conductivity is significantly lower, mainly caused by the treatment of the dam foundation (such as cement grouting).

4.2. Comparison with the field measurements

Fig. 7 shows the comparisons of the measured and calculated hydraulic heads at the piezometers installed close to the concrete–foundation interface. Among the piezometers, P12-2, P13-3 and P19-2 were installed in the boreholes drilled downwards from the drainage tunnels at the dam foundation. Influenced by the drainage hole array in the dam foundation, the measurements of these piezometers varied in a rather narrow range. Particularly, the measurements of P12-2 and P13-3 before March 2014 were only slightly higher than the floor elevation of the lowest drainage tunnels (about 1595 m) and varied consistently with the reservoir water level, with rather good agreement between the measurements and the numerical results. Afterwards, the correlation between the measurements and the reservoir water level disappeared and the measurements increased gradually. The reason for this change is not yet clear, and a possible explanation may be that some of the drainage holes near the water collecting well (with its location shown in Fig. 4a) were progressively clogged with fine-grained particles, which caused an increase of hydraulic head in the dam foundation close to the central cross-section. But as a result of the neighboring drainage holes that have been densely installed in the dam foundation, the clogged drainage holes only have a limited impact on the seepage flow in the local area, as evidenced by the measurements of the adjacent piezometers.

It can be further observed from Fig. 7 that the piezometers installed in the boreholes drilled downwards from the grouting tunnels (e.g. P6-1, P10-1, P11-2, P12-1, P13-2, P13-5, P13-6 and P16-6) have relatively higher readings as compared to the piezometers installed near the drainage holes, usually displaying a better correlation between the measurements and the reservoir water level. Nevertheless, the hydraulic head observations at these piezometers were still considerably lower than the reservoir water level, due to the reduction of pore water pressure in the foundation rocks by the grouting curtain and the drainage hole array.

Table 3
Back-calculated hydraulic properties of foundation rocks in zones Z_1–Z_6.

Foundation zone	Rock formation	Permeability (cm/s)
Z_1	$T_{2-3z}^{2(6)}$	7.2×10^{-5}
Z_2	$T_{2-3z}^{2(5)}$	4.6×10^{-5}
Z_3	$T_{2-3z}^{2(4)}$	5.3×10^{-5}
Z_4	$T_{2-3z}^{2(3)}$	2.2×10^{-5}
Z_5	$T_{2-3z}^{2(3)}$	5.8×10^{-5}
Z_6	$T_{2-3z}^{2(4)}$	8.7×10^{-5}

Fig. 8 shows the variations of the measured and calculated discharges into the drainage tunnel at 1595 m through the weirs WEDB-3 (at the left bank) and WEDB-4 (at the right bank). Overall, the numerical results seem to agree well with the measurements available before August 2013 (afterwards, no observations were available due to construction disturbance). The simulation results demonstrate that the discharges through weirs WEDB-3 and WEDB-4 varied consistently with the reservoir water level. But due to the better intactness of the foundation rocks and the draining effect caused by the underground powerhouse cavern system at the right bank, the discharge through weir WEDB-4 was much smaller than that through WEDB-3.

The numerical results also indicate that the discharges into the dam foundation mainly originate from the drainage tunnels at 1595 m and 1670 m. Fig. 9 plots the calculated discharges into the full length of the drainage tunnel at 1595 m at the left abutment and into the drainage tunnels at 1670 m. Chen et al. (2016) showed that the discharge into the drainage tunnel at 1595 m of the left abutment is relatively large due to the high permeability of rock formations $T_{2-3z}^{2(6)}$, $T_{2-3z}^{2(7)}$, and $T_{2-3z}^{2(8)}$, on which the abrupt decrease of the discharge on December 29, 2013 was induced by the closure of 29 drainage holes drilled in the drainage tunnel, an engineering treatment to the leakage problem. At the normal pool level of 1880 m, the total amount of discharge out of the drainage system in the dam foundation is about 55.5 L/s (50 L/s at the left bank and 5.5 L/s at the right bank), which agrees well with the magnitude of the field observations. The agreement between the simulation results and the observations of hydraulic head and discharge in the dam foundation implies that the back-calculated hydraulic conductivities and the specified boundary conditions are reliable and representative of the site characteristics.

4.3. Seepage flow behavior in the dam foundation

Based on the inverse results, the transient groundwater flow through the dam foundation can then be assessed with the PVI method. Figs. 10 and 11 plot the hydraulic head contours on the concrete–foundation interface and at the central cross-section of the dam on May 27, 2013, August 4, 2013 and August 26, 2014,

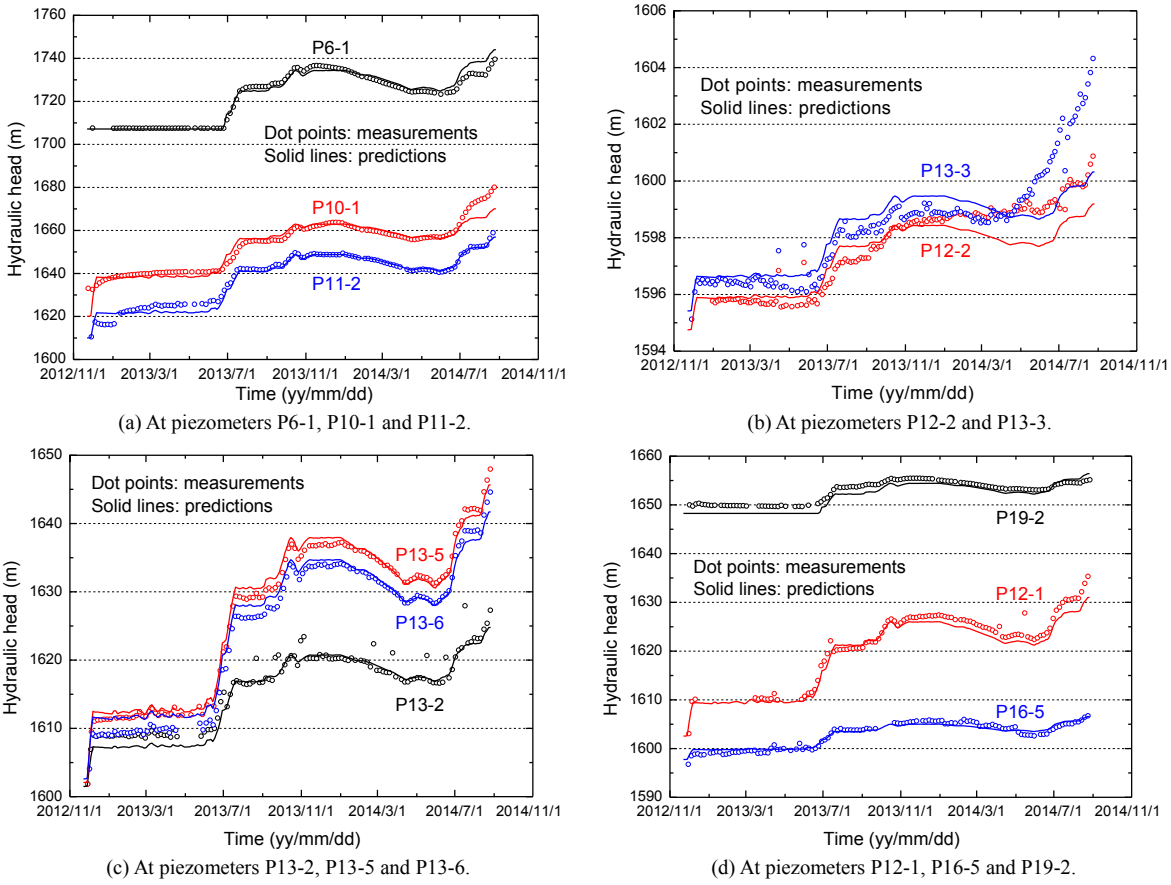

Fig. 7. Comparison of the measured and calculated hydraulic heads.

when the reservoir water level was about 1710 m, 1800 m and 1880 m, respectively. The results show that the hydraulic head on the upstream side of the grouting curtain increases gradually with the increase of the pool water level, but across the seepage-proof barrier and the drainage system, the hydraulic head decreases dramatically in the dam foundation. The grouting curtain bears a relatively larger water pressure difference compared to its surrounding rocks in the dam foundation, which is more significant when the normal pool level of 1880 m is attained. Downstream the seepage-proof barrier, the pore water pressure in the dam foundation (and the uplift pressure on the concrete–foundation interface) has been effectively lowered by the drainage hole array.

The numerical results indicate that the seepage control system consisting of the grouting curtain and the drainage holes and tunnels is effective in lowering the pore water pressure in and limiting the amount of discharge through the dam foundation, resulting in a dry zone in most part of the concrete–foundation interface downstream the drainage system even at the normal pool level (Fig. 10c). However, the construction of a massive concrete block for stabilizing the left bank abutment makes the distribution of hydraulic head at the left abutment quite different from that at the right abutment at the same elevation. Fortunately, the

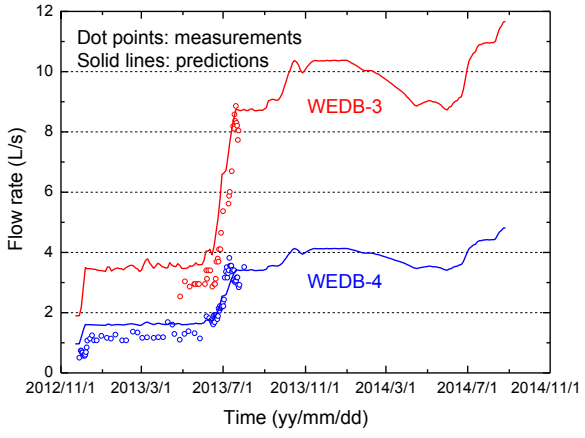

Fig. 8. Comparison of the measured and calculated discharges through the measuring weirs.

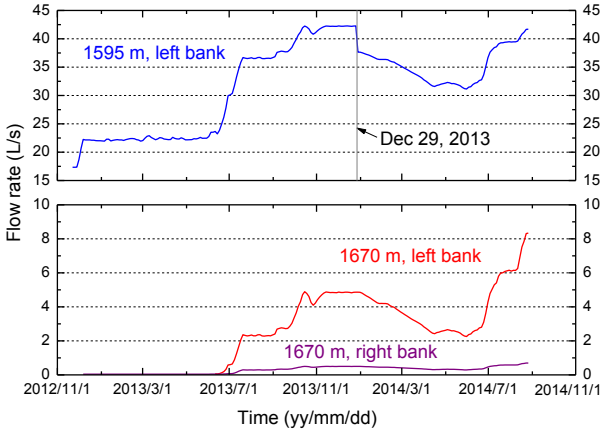

Fig. 9. Variation of the predicted discharges into the drainage tunnels.

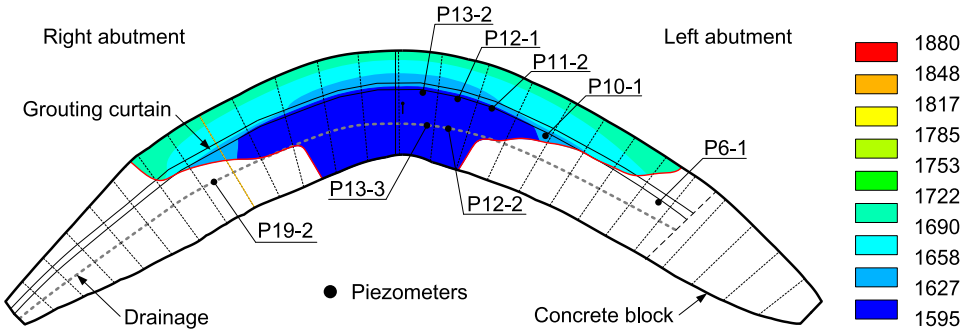

(a) On May 27, 2013 at pool water level of 1710 m.

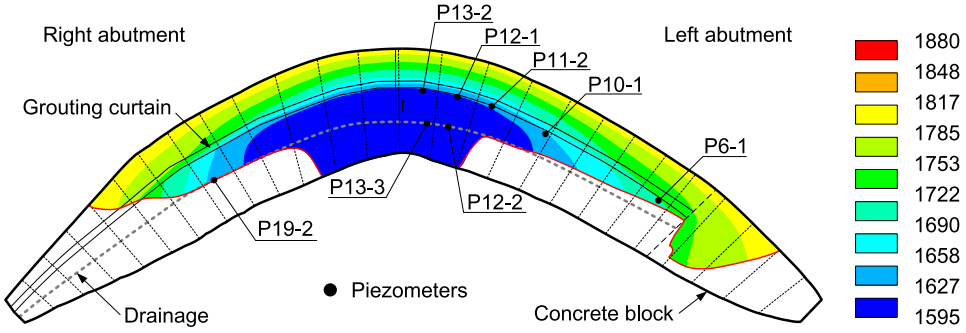

(b) On August 4, 2013 at pool water level of 1800 m.

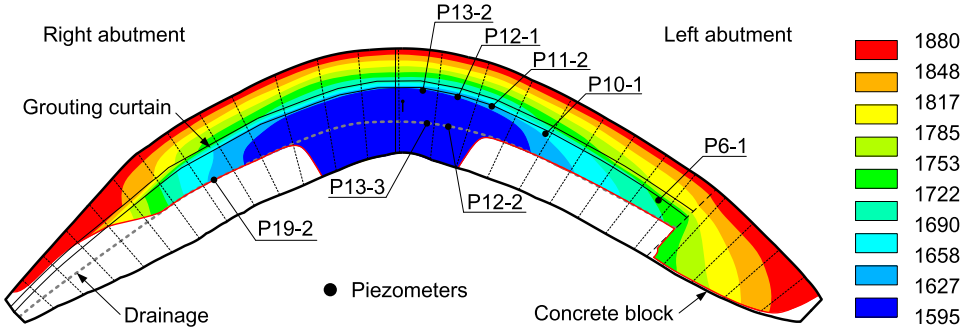

(c) On August 26, 2014 at pool water level of 1880 m.

Fig. 10. Hydraulic head contours at the concrete–foundation interface (unit: m).

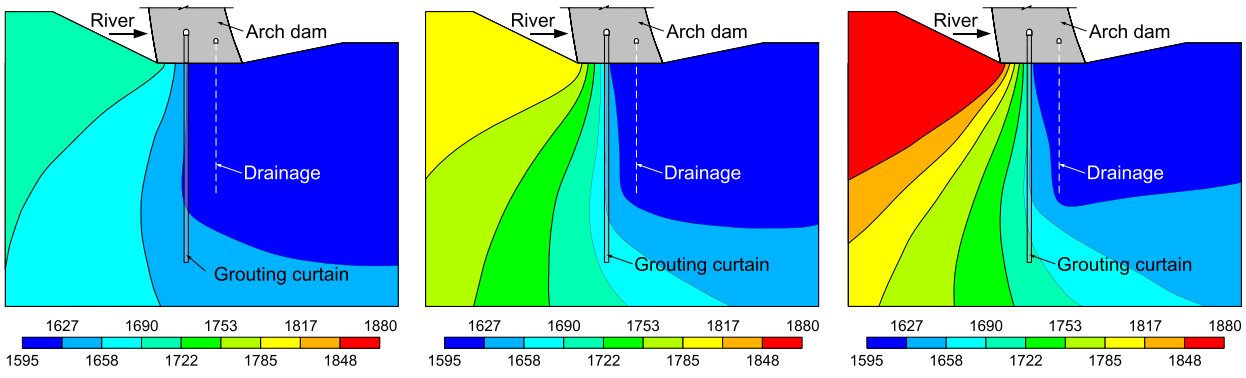

(a) On May 27, 2013 at pool water level of 1710 m. (b) On August 4, 2013 at pool water level of 1800 m. (c) On August 26, 2014 at pool water level of 1880 m.

Fig. 11. Hydraulic head contours at the central cross-section of the dam (unit: m).

numerical results suggest that the seepage flow in this concrete block has also been well controlled by the drainage system installed in the concrete block (Figs. 1 and 3).

5. Conclusions

This study systematically examined the permeability of the foundation rocks and the behaviors of transient groundwater flow in the Jinping I double-curvature arch dam foundation during the reservoir impounding stage. Based on the site characterization and borehole packer test results, the permeability of the foundation rocks close to the excavation surface that might be significantly influenced by the foundation excavation, treatment and concrete replacement was reassessed with an inverse modeling procedure using the time series measurements of discharge and hydraulic head. The inverse modeling procedure combines the methods of orthogonal design, transient groundwater flow modeling, artificial neural network and genetic algorithm-based optimization, which not only makes tractable the large-scale inverse problems in groundwater modeling, but also significantly improves the reliability of the inverse solutions. The inverse results suggest that the hydraulic conductivity of the foundation rocks at shallow depths is in the magnitude of $(2–9) \times 10^{-5}$ cm/s, which better represents the permeability of these rocks controlled by fracture patterns and influenced by engineering disturbances.

The numerical results, together with the field observations, show that the seepage control system consisting of the grouting curtain and the drainage holes and tunnels is effective in lowering the pore water pressure in and limiting the amount of discharge through the dam foundation. The hydraulic head decreases dramatically in the dam foundation across the seepage-proof barrier and the grouting curtain bears a relatively larger water pressure difference compared to its surrounding rocks in the dam foundation. Although the discharge into the drainage tunnel at 1595 m in the left abutment is relatively large, the total amount of discharge out of the drainage system in the dam foundation has been well controlled below 55.5 L/s.

Conflict of interest

The authors wish to confirm that there are no known conflicts of interest associated with this publication and there has been no significant financial support for this work that could have influenced its outcome.

Acknowledgments

The authors gratefully thank the anonymous reviewers for their constructive comments in improving this study. Financial supports from the National Natural Science Foundation of China (Grant Nos. 51579188 and 51409198) and the National Basic Research Program of China (Grant No. 2011CB013503) are gratefully acknowledged.

References

Ayvaz MT, Karahan H, Aral MM. Aquifer parameter and zone structure estimation using kernel-based fuzzy *c*-means clustering and genetic algorithm. Journal of Hydrology 2007;343(3–4):240–53.

Chai J, Wu Y, Li S. Analysis of coupled seepage and stress fields in rock mass around the Xiaowan arch dam. Communications in Numerical Methods in Engineering 2004;20(8):607–17.

Chang YC, Yeh HD, Huang YC. Determination of the parameter pattern and values for a one-dimensional multi-zone unconfined aquifer. Hydrogeology Journal 2008;16(2):205–14.

Chen Y, Zhou C, Zheng H. A numerical solution to seepage problems with complex drainage systems. Computers and Geotechnics 2008;35(3):383–93.

Chen Y, Zhou C, Jing L. Modeling coupled THM processes of geological porous media with multiphase flow: theory and validation against laboratory and field scale experiments. Computers and Geotechnics 2009;36(8):1308–29.

Chen Y, Hu R, Zhou C, Li D, Rong G, Jiang Q. A new classification of seepage control mechanisms in geotechnical engineering. Journal of Rock Mechanics and Geotechnical Engineering 2010;2(3):209–22.

Chen Y, Hu R, Zhou C, Li D, Rong G. A new parabolic variational inequality formulation of Signorini's condition for non-steady seepage problems with complex seepage control systems. International Journal for Numerical and Analytical Methods in Geomechanics 2011;35(9):1034–58.

Chen YF, Zheng HK, Wang M, Hong JM, Zhou CB. Excavation-induced relaxation effects and hydraulic conductivity variations in the surrounding rocks of a large-scale underground powerhouse cavern system. Tunnelling and Underground Space Technology 2015;49:253–67.

Chen YF, Hong JM, Zheng HK, Li Y, Hu R, Zhou CB. Evaluation of groundwater leakage into a drainage tunnel in Jinping-I arch dam foundation in Southwestern China: a case study. Rock Mechanics and Rock Engineering 2016;49(3):961–79.

Fan Q, Zhou S, Yang N. Optimization design of foundation excavation for Xiluodu super-high arch dam in China. Journal of Rock Mechanics and Geotechnical Engineering 2015;7(2):120–35.

Fei W, Zhang L, Zhang R. Experimental study on a geo-mechanical model of a high arch dam. International Journal of Rock Mechanics and Mining Sciences 2010;47(2):299–306.

Garcia LA, Shigidi A. Using neural networks for parameter estimation in ground water. Journal of Hydrology 2006;318(1–4):215–31.

Hernandez AF, Neuman SP, Guadagnini A, Carrera J. Inverse stochastic moment analysis of steady state flow in randomly heterogeneous media. Water Resources Research 2006;42(5). http://dx.doi.org/10.1029/2005WR004449.

Karahan H, Ayvaz MT. Transient groundwater modeling using spreadsheets. Advances in Engineering Software 2005a;36(6):374–84.

Karahan H, Ayvaz MT. Groundwater parameter estimation by optimization and dual reciprocity finite differences method. Journal of Porous Media 2005b;8(2):211–23.

Karahan H, Ayvaz MT. Simultaneous parameter identification of a heterogeneous aquifer system using artificial neural networks. Hydrogeology Journal 2008;16(5):817–27.

Li Y, Chen Y, Jiang Q, Hu R, Zhou C. Performance assessment and optimization of seepage control system: a numerical case study for Kala underground powerhouse. Computers and Geotechnics 2014;55:306–15.

Lin P, Zhou W, Liu H. Experimental study on cracking, reinforcement, and overall stability of the Xiaowan super-high arch dam. Rock Mechanics and Rock Engineering 2015;48(2):819–41.

Liu YR, Guan FH, Yang Q, Yang RQ, Zhou WY. Geomechanical model test for stability analysis of high arch dam based on small blocks masonry technique. International Journal of Rock Mechanics and Mining Sciences 2013;61:231–43.

Mao D, Yeh T, Wan L, Hsu K, Lee C, Wen J. Necessary conditions for inverse modeling of flow through variably saturated porous media. Advances in Water Resources 2013;52:50–61.

Qi S, Wu F, Yan F, Lan H. Mechanism of deep cracks in the left bank slope of Jinping first stage hydropower station. Engineering Geology 2004;73(1–2):129–44.

Virbulis J, Bethers U, Saks T, Sennikovs J, Timuhins A. Hydrogeological model of the Baltic Artesian basin. Hydrogeology Journal 2013;21(4):845–62.

Wang M, Chen YF, Hu R, Liu W, Zhou CB. Coupled hydro-mechanical analysis of a dam foundation with thick fluvial deposits: a case study of the Danba Hydropower Project, Southwestern China. European Journal of Environmental and Civil Engineering 2016;20(1):19–44.

Yang YS, Cronin AA, Elliot T, Kalin RM. Characterizing a heterogeneous hydrogeological system using groundwater flow and geochemical modelling. Journal of Hydraulic Research 2004;42(Suppl. 1):147–55.

Zhang L, Liu YR, Yang Q. Evaluation of reinforcement and analysis of stability of a high-arch dam based on geomechanical model testing. Rock Mechanics and Rock Engineering 2015;48(2):803–18.

Zhou XP, Zhang YX, Ha QL, Zhu KS. Micromechanical modelling of the complete stress–strain relationship for crack weakened rock subjected to compressive loading. Rock Mechanics and Rock Engineering 2008;41(5):747–69.

Zhou CB, Liu W, Chen YF, Hu R, Wei K. Inverse modeling of leakage through a rockfill dam foundation during its construction stage using transient flow model, neural network and genetic algorithm. Engineering Geology 2015;187:183–95.

Dr. Yifeng Chen is a professor in School of Water Resources and Hydropower Engineering, Wuhan University, China. He is a member of Chinese Society for Rock Mechanics and Engineering, and a committee member of Chinese Hydraulic Engineering Society for Rock and Soil Mechanics Specialized Committee. His research interests mainly cover rock mechanics and groundwater flow behaviors. Dr. Chen has managed over 10 projects funded by the National Natural Science Foundation of China and Ministry of Education of the People's Republic of China. In recent years, he has been particularly devoted to groundwater flow behaviors and their control in foundation rocks of dams and surrounding rocks of caverns in large-scale hydropower projects. To date, he has published about 100 journal papers.